Benefits of assimilating thin sea-ice thickness from SMOS into the TOPAZ system

Jiping Xie[1], Francois Counillon[1], Laurent Bertino[1], Xiangshan Tian-Kunze[2], and Lars Kaleschke[2]

1. Nansen Environmental and Remote Sensing Center, Bergen, Norway
2. Institute of Oceanography, University of Hamburg, German

Abstract An observation product for thin sea ice thickness (SMOS-Ice) is derived from the brightness temperature data of the European Space Agency's (ESA) Soil Moisture and Ocean Salinity (SMOS) Mission, and is available in real-time at daily frequency during the cold season. In this study, we investigate the benefit of assimilating SMOS-Ice into the TOPAZ system. TOPAZ is a coupled ocean-sea ice forecast system that assimilates SST, altimetry data, temperature and salinity profiles, ice concentration, and ice drift with the Ensemble Kalman Filter (EnKF). The conditions for assimilation of sea ice thickness thinner than 0.4 m are favorable, as observations are reliable below this threshold and their probability distribution is comparable to that of the model. Two parallel runs of TOPAZ have been performed respectively in March and November 2014, with assimilation of thin sea ice thickness (thinner than 0.4 m) in addition to the standard ice and ocean observational data sets. It is found that the Root Mean Square Difference (RMSD) of thin sea-ice thickness is reduced by 11% in March and 22% in November suggesting that SMOS-Ice has a larger impact during the beginning of freezing season. There is a slight improvement of the ice concentrations and no degradation of the ocean variables. The Degrees of Freedom for Signal (DFS) indicate that the SMOS-Ice contains important information (> 20% of the impact of all observations) for some areas in the Arctic. The areas of largest impact are the Kara Sea, the Canadian archipelago, the Baffin Bay, the Beaufort Sea and the Greenland Sea. This study suggests that SMOS-Ice is a good complementary data set that can be safely included in the TOPAZ system as it improves the ice thickness and the ice concentration but does not degrade other quantities.

Keywords: SMOS-Ice; EnKF; thin sea-ice thickness; Degrees of Freedom for Signal; Observing System Experiment;

1. Introduction

The Arctic climate system has undergone large changes during the last 20 years: increase of temperature (Chapman and Walsh, 1993; Serreze et al., 2000; Karl et al., 2015; Roemmich et al., 2015), decrease of sea ice extent (Johannessen et al., 1999; Shimada et al., 2006;), sea ice thinning and loss of sea ice volume (Rothrock et al., 1999; Kwok and Rothrock, 2009; Laxon et al., 2013). The interpretation of such changes is severely hampered by the sparseness and the diversity of observational network. The reanalysis database that combines the sparse observations with dynamically consistent models is becoming an important tool.

While observations of sea ice concentrations have been available for the past 30 years, observations of sea ice thickness are comparatively sparse. An improved knowledge of the ice thickness would be greatly beneficial both for model developments and for improving the accuracy of operational ocean forecasting system. The initialization of sea-ice thickness is also expected to improve predictability on seasonal time scale (Guemas et al. 2014). Until the last decade, observations of sea-ice thickness were mostly limited to field campaigns or submarine measurements. Major efforts in remote sensing have been proposed to monitor the spatiotemporal evolution of ice thickness, and gradually obtained various products from different satellite retrieval algorithms. Measurements of thick sea ice freeboard on basin-wide scales have been derived from laser altimeters on board ICESat (e.g., Forsberg and Skourup, 2005; Kurtz et al., 2009; Kwok and Rothrock, 2009) or from radar altimeters on ERS, EnviSAT and CryoSat2 (e.g., Laxon et al., 2003; Giles et al., 2007; Connor et al., 2009). Still large uncertainties remain in the accuracy of the resulting ice thickness estimates (larger than 0.5 m) due to uncertainties in the snow depth and the sea ice density (Zygmuntowska et al., 2014). A new database based on Cryostat2 has been provided (Laxon 2013; Ricker et al., 2014) and has been made available in near real time (Tilling et al. 2016). Finally, methods for sea ice thickness retrieval based on measurements of the brightness temperature at a low microwave frequency of 1.4 GHz (L-band: wavelength λ_a=21 cm) have been developed in preparation for the European Space Agency's

(ESA) Soil Moisture and Ocean Salinity (SMOS) mission (Heygster et al., 2009; Kaleschke et al., 2010). It has been shown that SMOS can be used to retrieve level ice thickness up to half a meter under cold conditions (Kaleschke et al., 2012; Huntemann el al., 2014).

An improved retrieval method based on a radiative transfer model and a thermodynamic sea ice model has been further proposed by considering the variations of ice temperature, salinity and a statistical thickness distribution (Tian-Kunze et al., 2014). The operational daily product derived using this method, henceforth called SMOS-Ice, has been validated during a field campaign in the Barents Sea (Kaleschke et al., 2016; Mecklenburg et al., 2016) and will be used in this study. Aiming at the operational application of the thickness measurements for sea ice, the SMOS-Ice data contain daily products of sea ice thickness since October 2010 (Tian-Kunze et al., 2014).

Yang et al. (2014) studied the benefit of assimilating SMOS-Ice during the freezing period, with the Localized Singular Evolutive Interpolated Kalman filter (LSEIK, *ref*. Nerger et al., 2005) in a nested Arctic configuration of the MITgcm. They found that SMOS-Ice leads to improvement of ice thickness and ice concentration. The present study follows up the work from Yang et al. (2014) but uses a different model and assesses: 1) the impact of assimilating SMOS-Ice both during the beginning of the melting and freezing seasons; 2) the relative contribution of SMOS-ice compared to a complete set of observations typically used in a state of the art forecasting system.

The TOPAZ system is a coupled ocean-sea ice data assimilation system that focuses on the marine environment in the Arctic region. It is the operational Arctic forecast system in the Copernicus Marine Services (http://marine.copernicus.eu/). The system provides 10-days coupled physical-biogeochemical forecast every day and long-term reanalysis (Sakov et al., 2012; Lien et al., 2016; Xie et al., 2016). At present, the TOPAZ system assimilates the Sea Surface Temperature (SST), along-track Sea Level Anomalies (SLA) from satellite altimeters, in situ temperature and salinity profiles, Sea Ice Concentration (ICEC) and sea

ice drift data from satellites with the Ensemble Kalman Filter (EnKF). The reanalysis product of the TOPAZ system has been widely used in studies about ocean circulation and sea ice in the northern Atlantic Ocean or in the Arctic region (Melsom et al., 2012; Johannessen et al., 2014; Korosov et al., 2015; Lien et al., 2016). However, TOPAZ does not assimilate sea ice thickness, although the capability has been demonstrated in Lisæter et al. (2007). TOPAZ does not apply post-processing for this variable. In the Arctic reanalysis for the period 1991-2013, the daily sea ice thickness of TOPAZ has been validated and compared to different types of available observations (Xie et al., 2016). TOPAZ shows good agreement with the spatial distribution of ice thickness in ICESat data (available between 2003 and 2008) with a spatial correlation 0.74 in spring and 0.84 in autumn. However, TOPAZ shows a clear overestimation of ice thickness in the Beaufort Sea and an underestimation in other areas of the Arctic. Inaccuracies in the ice thickness are a common limitation of coupled ice-ocean models in the Arctic (Johnson et al., 2012; Schweiger et al., 2012; Smith et al., 2015).

This paper is organized as follows: section 2 introduces the main components of TOPAZ system including the model, the assimilation scheme, and the observations assimilated. In section 3, we compare SMOS-ice data to the TOPAZ reanalysis for the period 2010-2013, to investigate potential biases and whether conditions are favorable for data assimilation. In section 4, an Observing System Experiment (OSE) is conducted, consisting of two assimilation runs with and without the SMOS-Ice data during 2014. In Section 5, we compared the contributions of SMOS-Ice relative to other types of observations.

2. Descriptions of TOPAZ data assimilation system

2.1 The coupled ice-ocean model

The ocean general circulation model used in the TOPAZ system is the version 2.2 of the Hybrid Coordinate Ocean Model (HYCOM) developed at University of Miami (Bleck, 2002; Chassignet et al., 2003). HYCOM uses a hybrid vertical coordinate, which smoothly transits from isopycnal layers in the stratified open ocean to z-level coordinates in the unstratified

surface mixed layer. This feature has been demonstrated in a wide range of applications from the deep oceans to the shelf (Chassignet et al., 2009). The NERSC-HYCOM model is coupled to a one-thickness category sea-ice model, for which the ice thermodynamics are described in Drange and Simonsen (1996) and the ice dynamics are based on the elastic-viscous-plastic rheology described in Hunke and Dukowicz (1997) and with a modification from Bouillon et al. (2013). The TOPAZ grid uses conformal mapping (Bentsen et al., 1999) and has a quasi-homogeneous horizontal resolution of 12-16 km in the Arctic as shown in Fig. 1.

The temperatures and salinities at model lateral boundaries are relaxed to a combined climatology using the World Ocean Atlas of 2005 (WOA05, Locarnini et al., 2006) and the version 3.0 of the Polar Science Center Hydrographic Climatology (PHC, Steele et al., 2001). A seasonal inflow from the Pacific Ocean through the Bering Strait is imposed, which amplitude is following the observations from Woodgate et al. (2012).

2.2 Implementation of the EnKF in TOPAZ

The analysis field at time *t* with the standard EnKF, is expressed as follows:

$$\mathbf{x}^{\mathrm{a}} = \mathbf{x}^{\mathrm{f}} + \mathbf{K}\left(\mathbf{y} - \mathbf{H}\mathbf{x}^{\mathrm{f}}\right), \quad (1).$$

where **x** is the model state vector, the superscripts “a” and “f” refer to the analysis and the forecast respectively. The ensemble consists of 100 dynamical members. **H** is the observation operator and **y** is the observation vector, which includes all observations at the assimilation time window. The term innovation refers to the misfits between the observations and the model: *i.e.* the term in bracket in equation (1). The Kalman gain **K** in Equation (1) is calculated as:

$$\mathbf{K} = \mathbf{P}^{\mathbf{f}}\mathbf{H}^{\mathbf{T}}[\mathbf{H}\mathbf{P}^{\mathbf{f}}\mathbf{H}^{\mathbf{T}} + \mathbf{R}]^{-\mathbf{1}} \quad (2).$$

Where **R** is the matrix of observation error variance, and $\mathbf{P}^{\mathrm{f}}$ is the matrix of background error covariance, calculated as $\mathbf{P}= (1/N\text{-}1)*\mathbf{A}\mathbf{A}^{\mathrm{T}}$ where *N* is the number of ensemble members, the superscript T denotes a matrix transpose, and **A** is the ensemble of anomaly which can be calculated as:

$\mathbf{A}^{\mathrm{f}} = \mathbf{X}^{\mathrm{f}} - \overline{\mathrm{x}^{\mathrm{f}}}\mathrm{I}_{N}$,

where $\mathbf{X}^{\mathrm{f}}$ denotes the matrix of the forecastd model states, $\overline{\mathrm{x}^{\mathrm{f}}}$ is the ensemble average of the state vector, and $\mathrm{I}_N = [1, \ldots, 1]$ is the vector with all components equal to 1. The TOPAZ system uses the deterministic EnKF (DEnKF, Sakov and Oke, 2008; Sakov et al., 2012), which is a square-root filter implementation of the EnKF that solves the analysis without the need for perturbation of the observations. The DEnKF overestimates the analysed error covariance by adding a semi-definite positive term to the theoretical error covariance given by the Kalman filter, which mitigates the need for inflation (Sakov and Oke, 2008). The ensemble mean is updated by the equation:

$$\overline{\mathbf{x}^{\mathbf{a}}} = \overline{\mathbf{x}^{\mathrm{f}}} + \mathbf{K}(\mathbf{y} - \mathbf{H}\overline{\mathbf{x}^{\mathbf{f}}}),$$

and the ensemble anomaly is calculated as follows:

$$\mathbf{A}^{\mathbf{a}} = \mathbf{A}^{\mathbf{f}} - \frac{\mathbf{1}}{\mathbf{2}}\mathbf{K}\mathbf{H}\mathbf{A}^{\mathbf{f}}.$$

Finally, the element states of the ensemble are reconstructed by adding the two terms as follows:

$$\mathbf{X}^{\mathrm{a}} = \mathbf{A}^{\mathrm{a}} + \overline{\mathbf{x}^{\mathrm{a}}}\mathrm{I}_N \quad (3)$$

where $\mathbf{X}^{\mathrm{a}}$ represents the matrix of the updated model states after data assimilation.

An overview of the observations assimilated in the present TOPAZ system is given in Table 1 (see as well Sakov et al, 2012). Observations are quality-controlled and superobed as in Sakov et al (2012). The system assimilates the following data sets on a weekly basis: the gridded OSTIA SST (Donlon et al., 2012); OSI-SAF ice concentration available for the analysis day; along-track Sea Level Anomaly; delayed-mode profiles of temperature and salinity, and the sea-ice drift during the 3 days prior to the analysis. All measurements are retrieved from http://marine.copernicus.eu. The SLA data and the sea ice drift data are assimilated asynchronously (See Sakov et al., 2010)

3. Bias analyses for thin ice thickness in TOPAZ

TOPAZ provides a reanalysis at daily frequency of physical variables including sea ice thickness, which was validated by in situ and satellite observations in Xie et al. (2016). An assumption made for data

assimilation is that the model and observations have unbiased mean and uncertainties estimates. Therefore, we investigate in this section the thickness misfits of thin sea ice during five cold seasons of 2010-2014.

SMOS-Ice products (version 2.1) are available since 2010 in the cold season from 15th October to 15th April. They are provided by Hamburg University at the website of https://icdc.zmaw.de/1/daten/cryosphere/l3c-smos-sit.html (Kaleschke et al., 2012; Tian-Kunze et al., 2014). SMOS sea ice thickness maps are provided at daily frequency from October 2010 and are available in near-real time during the cold season.

The sea ice thickness of TOPAZ is extracted from the model state on daily average, and then compared with the observations by calculating the bias and the Root Mean Square Difference (RMSD) as follows:

$$\mathbf{Bias} = \frac{1}{n}\sum_{i=1}^{n}(\mathbf{H}_i\bar{\mathbf{x}}_i^{\mathrm{f}} - \mathbf{y}_i) \quad (4)$$

$$\mathbf{RMSD} = \sqrt{\frac{1}{n}\sum_{i=1}^{n}(\mathbf{H}_i\bar{\mathbf{x}}_i^{\mathrm{f}} - \mathbf{y}_i)^2}\,, \quad (5)$$

where $\bar{\mathbf{x}}_i^{\mathrm{f}}$ is the daily averaged model state that is compared to the observation at the same location and time, **H** is the observation operator similar with that in the equation (1), and *n* is the number of available observations in the compared time period.

Figure 2 shows the TOPAZ ice thickness as conditional expectations with respect to SMOS-Ice data sorted into 5 cm bins. The TOPAZ ice thicknesses shown in Fig.2 are at the same locations and times as the observations. Overall, the sea ice thickness in TOPAZ tends to be overestimated but it varies with the month and with the amplitude of ice thickness (more pronounced for thick ice). As an example, TOPAZ overestimates the high thickness values (>0.4 m) during October and February-April, while those are underestimated in November. For thicknesses lower than 0.4 m, the match between the observations and the simulations of TOPAZ is closer and rather consistent through the cold season. There is no clear bias from October–December but an increasing thick bias from January-April. There is no a priori indication whether the bias is a model bias or an observation bias. The penetration depth into sea ice is about 0.5 m for the L-Band microwaves frequency (Kaleschke

et al., 2010; Huntemann et al., 2014), and the effect of ice melting may lead to a saturation thickness of less than 0.4 m (see Heygster et al. (2009)). In order to avoid multivariate transfers of bias (whichever the source) to other state variable during the multivariate assimilation of SMOS-Ice, we only retain thickness observations that are less than 0.4 m.

In Fig. 3, we estimate the yearly bias of ice thickness compared to SMOS-Ice for ice that is thinner than 0.4 m over the period 2010-2014. After 2011, the thick bias is increased, and reaches a maximum of 0.1 m in 2014. The thick bias in March is also found larger than in November. There is a large spatial variability in the distribution of the bias (right panel of Fig.3), with the bias being largest in the Beaufort Sea and in the Kara Sea. In 2014, there is a thick bias in all the regions,

4. Observing System Experiment of SMOS-Ice

4.1 Design of OSE runs for SMOS-Ice

The SMOS-Ice ice thickness data is gridded at a resolution of approximately 12.5 km and available at daily frequency in the cold season. Only the observations between 0 and 0.4 m, with a distance of at least 30 km away from the coast are used (See Section 3). The innovations in Equation (1) are expressed as a sea ice volume, which is an additive variable suited for spatial interpolation:

$$\Delta\mathbf{hice} = \mathbf{y}_{\mathrm{smos}} - \mathbf{H}(\mathbf{h}_{\mathrm{mod}} \times \mathbf{f}_{\mathrm{mod}}), \qquad (6)$$

where $\mathbf{y}_{\mathrm{smos}}$ is the observed thickness of thin sea ice from SMOS-Ice, **H** is the same interpolation as in equation (1), $\mathbf{h}_{\mathrm{mod}}$ and $\mathbf{f}_{\mathrm{mod}}$ are the model sea ice thickness and concentration respectively. To highlight the additional impacts of observations, two assimilation runs for Observing System Experiment (OSE) are carried out:

- **Official Run**: uses the standard observational network of the TOPAZ system. It assimilates every week the along-track Sea Level Anomaly, SST, in situ profiles of temperature and salinity, sea-ice concentrations and sea-ice drift data (listed in **Table** 1).
- **Test Run**: assimilates the SMOS-Ice data in addition to observations assimilated in the official run. The observation error (related with the **R**

term in Eq. (2)) of the sea ice thickness uses the uncertainties recommended by the provider, with an upper limit of 5 m beyond which the observations are assumed fully saturated. This uncertainty is an a priori estimate of the maximum uncertainty with respect to variations in the input parameters TB, T_{ice} and S_{ice} (Tian-Kunze et al., 2014). Here, the observation error is assumed spatially uncorrelated.

We have two parallel assimilation runs focusing on two typical time periods within the beginnings of ice melting and freezing, from 19th February to 31st March and from 22nd October to 30th November in 2014. Both runs are driven by the same atmospheric high frequency forcing from ERA-Interim (Dee et al., 2011). Finally, the daily averaged outputs in March and November are used for the evaluation.

4.2 Error analysis in the OSE runs

The error analysis focuses on the following target quantities: sea ice thickness, sea ice concentration, SST and SLA. All quantities are derived from daily averages at same observation locations and time, and the calculation of the bias and the RMSD is according to equations (4) and (5) respectively.

The spatial distribution of selected SMOS-Ice data for thin sea ice is shown in the top panels of Fig. 4 during March and November of 2014. In March, the available observations in the Beaufort Sea are very few, and unevenly distributed - mainly located in the coastal estuary areas. During this period, most of the observations are unreliable in the Beaufort Sea (with errors saturated at 5 m) so that they are rejected. Therefore in the following analysis, we will only present the result in November for the Beaufort Sea. In the middle panels of Fig. 4, the differences of RMSD for sea-ice thickness between the Official Run and the Test Run are shown (red color indicates an improvement due to assimilation of SMOS-Ice). In March, the improvements are mainly found to the east of Franz Josef Land and to some extent near the ice edge in the Greenland Sea. In November, the reduction of RMSD is larger than 0.2 m in the Beaufort Sea, the Greenland Sea and to the North of Svalbard. Finally, the differences of monthly ice thickness between the Official Run and the

Test Run are shown in the bottom panels of Fig. 4. It suggests that assimilating SMOS-Ice leads to a reduction of sea-ice thickness both in March and November 2014.

The time series of daily bias and RMSD for thin ice thicknesses in the OSE runs are shown in the top panels of Fig. 5. The bias of thin sea-ice thickness is reduced from 16 cm to 12 cm in March, and from 7 cm to 4 cm in November, when SMOS-Ice data is assimilated. The RMSD of thin sea ice is reduced from 35 cm to 31 cm in March, and from 27 cm to 21 cm in November. This corresponds to a reduction of the bias of 25% in March and 43% in November, and a reduction of the RMSD of about 11% in March and 22% in November. In the other panels of Fig. 5, the bias and RMSD of sea ice concentration, SST and SLA are presented. There is a slight benefit for the bias and RMSD of sea ice concentration, but the statistics for SST and SLA are unchanged.

Moreover, the averaged thicknesses of thin sea-ice in the marginal seas - in the Kara Sea, Barents Sea and Beaufort Sea - are shown with marked lines in the panels of Fig. 6. The corresponding daily RMSDs of ice thickness relative to thin SMOS-Ice data are added with shading. In each month, there are four assimilation steps marked with vertical lines.

In the Kara Sea, the thickness observed in March is very stable with a slight gradual increase. There is a relatively uniform reduction of RMSD by about 21%, which is mainly the result from a correction of the large (too thick) bias in the model. In November, the bias is much smaller and the resulting improvement is smaller (8%) but the performances are slightly improving through the month for RMSD.

In the Barents Sea, in March, the observations show an increasing trend. The official run shows initially a large (thick) bias that reduces as the thickness increases in the observations. Assimilation of SMOS-Ice data reduces well the initial bias, but the bias converges towards the official run at the end of the month and so is the RMSD. On average, the RMSD of ice thickness is decreased about 27% from the Test Run. In November, the observations show large variability that is well captured in the Official Run but the ice is initially too thick. The RMSD reduction is about 19%

from the Test Run compared to from the Official Run and both the bias and the variability seem to be reduced.

In the Beaufort Sea, there are too few observations to provide a representative estimate of the system performance in March (top panels of Fig. 4) and the statistics are not presented. In November, the observations show an increasing trend and the official run shows once again a relatively large thick bias initially. The RMSD in the Test Run is reduced by about 51%, which is mainly caused by a reduction of the bias. The increasing trend in the Test Run is in relatively good agreement with the observations.

In Fig 7, we are validating the ice thickness with independent sea-ice thickness observations from two buoys (*2013F* and *2014F)*. During the month of November 2014, their drift trajectories are shown in the right panels of Fig. 4. These measurements are estimated from the autonomous Ice Mass Balance buoys (IMP; http://imb.erdc.dren.mil/buoyinst.htm) respectively located at (158.41°W, 77.63°N) and (146.34°W, 76.71°N) on the 1st November 2014. The RMSDs of ice thickness of the OSE runs are shown with the dashed blue and crossed red lines in Fig. 7. Along the buoy trajectory, the daily series of the observed sea ice thickness from 21st October to 30th November are shown with the blue squared line and the standard deviation is shown with error bars. The overestimation of sea ice thickness in the Official Run is slightly reduced (with a maximum decrease of 2 cm). It is expected that the impact of SMOS-ice on the two buoys are small because they are located far away from location where SMOS-Ice data is assimilated (shown as the top row panel in Fig. 4). Note that the TOPAZ assimilation system uses localization, meaning that the impact of observations is limited to a certain radius and their influence reduces as function of distance. In TOPAZ the effective localization radius is 90 km. It is encouraging to see that the improvement seems to be increasing with time suggesting that the region influenced by SMOS-ice is gradually spreading with time.

5. Relative impact of SMOS-ice to the existing observation network

In this Section, the additional benefit of assimilating SMOS-Ice into the TOPAZ system is compared quantitatively with respect to the standard observation network. To do so, we evaluate a performance metric calculated during the analysis, the Degree of Freedom for Signal (DFS), which is widely used for such purposes (Rodgers 2000; Cardinali et al. 2004). During the assimilation, one can calculate the DFS as follows:

$$\mathrm{DFS} = tr\left(\frac{\partial \hat{\mathbf{y}}}{\partial \mathbf{y}}\right) = tr\left\{\frac{\partial[\mathbf{H}(\mathbf{X}^{\mathrm{a}})]}{\partial \mathbf{y}}\right\} = tr(\mathbf{KH}) \quad (7).$$

Here, the matrix **K** and the observation operator **H** are the same as in equation (1), and *tr* defines the trace, applied to the matrix (**KH**). The DFS measures the reduction of mode that can be attributed to each observation type. A value of DFS close to 0 means that the observation has no impact, while a value of *m* means that the assimilation has reduced the number of degree of freedom of the ensemble by *m*. Note that the reduction cannot exceed the ensemble size; i.e. 100 here. In Sakov et al. (2012), it was recommended that the DFS should not exceed 10 % of the ensemble size to avoid a collapse of the ensemble.

After each data assimilation time *i*, the DFS of the *j*'th type of observations can be calculated by equation (7), denoted DFS_{ij}. Given an observation type, the averaged DFS over a specific time period can be estimated by:

$$\overline{\mathrm{DFS}_j} = \frac{1}{m}\sum_{i=1}^{m} \mathrm{DFS}_{ij}, \quad (8).$$

where the subscript *j* represents the j^{th} observation data set assimilated, the subscript *i* is for the time and *m* is the total number of assimilation steps within the time period considered (here 4). Since the assimilation is performed locally, the DFS values are obtained at each model grid cell. In Fig. 8, we are plotting the averaged DFS maps (as defined in Eq. 8) for the different observation data set assimilated in March and November. In the Arctic the total DFS is dominated by the ice concentration with large value near the ice edge. The DFS for SMOS-Ice is comparatively small. It is larger in March than in November. However, in some regions, the monthly DFS of SMOS-ice reaches values larger than 2.

Furthermore, based on the sum of the DFS of all observation types assimilated in TOPAZ, we can estimate the relative impact the *j*'th type of observations ($RDFS_j$):

$$\mathrm{RDFS}_j = \frac{\overline{\mathrm{DFS}}_j}{\sum_{l=1}^{O} \overline{\mathrm{DFS}}_l} \times 100\%, \quad (9)$$

where *O* is total number of observation types. Figures 9 and 10 show the relative contribution of each observational data set. As expected, the assimilation of ice concentration dominates the total DFS, while the impacts of SST and SLA are limited to the region that are not ice covered. Ocean temperature and salinity profiles near the North Pole in the Arctic are the Ice-Tethered Profiles (ITP), which are collected by the Ice-Tethered Profiler Program (Krishfield et al., 2008; Toole et al., 2011). They have a very large impact but they are very sparse. In March the SMOS-ice data has a significant impacts (> 20 % of the total DFS) in the Northern Barents Sea, the Western Kara Sea, Baffin Bay, the Greenland Sea and in Hudson Bay. In November, the relative contribution is still large in the Barents Sea, the Kara Seas and in the Greenland Sea, but it is now also large in the Beaufort Sea and in the Canadian Archipelago.

6. Summary and Discussion

The thickness observations of thin sea ice in the Arctic can be derived from SMOS brightness temperature at 1.4 GHz (Tian-Kunze, et al., 2014; Kaleschke et al., 2016). This data set is available in near real time since 2010 at daily frequency. This study investigates the impact of assimilating this data set within the TOPAZ system, which is the Arctic component of the Copernicus Marine Services. It is shown that for thin ice (less than 0.4 m), the TOPAZ reanalysis and the SMOS-Ice have comparable distributions, but TOPAZ reanalysis tends to overestimate thin ice thickness, especially from January to April.

We compare the benefit of assimilating SMOS-ice (thinner than 0.4 m) in TOPAZ system that already assimilates ice concentration, SST, SSH and temperature and salinity profiles. The comparison is carried out for two periods: February-March and October-November of 2014. The study shows that the assimilation of SMOS-Ice data reduces the thickness

RMSD of thin sea-ice in March and in November by about 11% and 22% respectively, mainly caused by the reduction of the bias (too thick sea ice that seems larger in 2014 than in previous years). As in Yang et al. (2014) we also find that there is a slight improvement to the ice concentration. The RMSDs for SST and SLA remain unchanged but they are at least not degraded.

In this study, the DFS has been used to evaluate the relative contributions of assimilated observations to the reduction of error in the TOPAZ system. The SMOS-Ice data have a smaller impact than ice concentration, but a relatively high contribution in some areas. In the Greenland Sea, the Kara Sea and the Barents Sea, a significant contribution (defined as larger than 20 % of the total impact from all observations) is found both in March and November. In Baffin Bay and Hudson Bay, significant contributions are also found in March. In November, there is a large contribution in the Beaufort Sea and in the Canadian archipelago.

To conclude, we found that the assimilation of SMOS-ice can reduce the thick biases in some regions of the Arctic. It is also encouraging that the assimilation of this data set does not degrade other variables (SST, SLA, ICEC and ice drift). This suggests that SMOS-Ice can be assimilated without degradation of other skills in the operational forecasting system and included in reanalysis mode. However, further work needs to be done to better understand the uncertainty of the assimilated sea ice thickness from the SMOS-Ice. Recently, Yang et al. (2016) tested the sensitivity of assimilating the SMOS-Ice data with the LSEIK during the winter of 2011-2012, and found that perturbations of the atmospheric forcing is important for improving the performance of assimilation, consistently with the findings of Lisæter et al. (2007).

In the future, we may use the “saturation ratio” that is defined by the relationship of the variable L-band penetration depth and the maximal retrieval thickness as a function of temperature and salinity with which we can better identify the valid observations of sea ice thickness from SMOS. In addition, the satellite CryoSat2 provides freeboard height data in thick ice that can complement the observations from SMOS (Kaleschke et al.,

2010). The new sea ice thicknesses derived from a combination of SMOS and CryoSat2 will be soon available (Kaleschke et al., 2015). Incidentally, the U.S Navy Arctic Cap Nowcast/Forecast System (ACNFS) is currently testing the assimilation of a combined sea ice thickness product where the sea ice thickness is blended from SMOS-Ice and CryoSat2 based on each satellite retrieval error (personal communication from David Hebert). Where the ice is thin (typically less than 0.5 m), the relative error for SMOS-Ice will be lower than CryoSat2, and the blending will be weighted strongly toward the thickness value from SMOS-Ice. Where the ice is thick, the error will be lower for CryoSat2 retrieval and the blending will be strongly weighted toward the CryoSat2 ice thickness value.

Acknowledgment

The authors are grateful to two anonymous reviewers for their insightful comments that were helpful in improving the paper. Thanks to Dr. Y. Wang for useful discussions. This study was supported by ESA contracts 4000101476/10/NL/CT and 4000112022/14/I-AM and CPU time from the Norwegian Supercomputing Project (NOTUR II grant number nn2993k).

Reference:

Bentsen, M., Evensen, G., Drange, H., and Jenkins, A. D.: Coordinate transformation on a sphere using conformal mapping, Mon. Weather Rev., 127, 2733–2740, doi:http://dx.doi.org/10.1175/1520-0493(1999)127<2733:CTOASU>2.0.CO:2, 1999.

Bleck, R.: An oceanic general circulation model framed in hybrid isopycnic-Cartesian coordinates, Ocean Model., 4, 55–88, doi:10.1016/S1463-5003(01)00012-9, 2002.

Bouillon, S., Fichefet, T., Legat, V., and Madec, G.: The elastic-viscous-plastic method revised. Ocean Modell. 7, 2-12. doi:10.1016/j.ocemod.2013.05.013, 2013.

Cardinali, C., Pezzulli, S., and Andersson, E.: Influence-matrix diagnostic of a data assimilation system, Q. J. R. Meteorol. Soc., 130, 2767–2786, doi:10.1256/qj.03.205, 2004.

Chapman, W. L., and Walsh, J. E.: Recent variations of sea ice and air temperature in high latitudes, Bull. A mer. Meteorol. Soc., 74, 33 —47, doi: http://dx.doi.org/10.1175/1520-0477(1993)074<0033:RVOSIA>2.0.CO:2, 1993.

Chassignet, E. P., Hurlburt, H. E., Metzger, E. J., et al.: US GODAE: Global Ocean Prediction with the HYbrid Coordinate Ocean Model (HYCOM), Oceanography, 22, 64–75. Doi:10.5670/oceanog.2009.39, 2009.

Chassignet, E. P., Smith, L. T., and Halliwell, G. R.: North Atlantic Simulations with the Hybrid Coordinate Ocean Model (HYCOM): Impact of the vertical coordinate choice, reference pressure, and thermobaricity, J. Phys. Oceanogr., 33, 2504–2526. Doi: http://dx.doi.org/10.1175/1520-0485(2003)033<2504:NASWTH>2.0.CO:2, 2003.

Connor, L. N., Laxon, S. W., Ridout, A. L., Krabill, W. B., and McAdoo, D. C.: Comparison of Envisat radar and airborne laser altimeter measurement over Arctic sea ice. Remote Sensing of Environment. 113, 563-570,

dio:10.1016/j.rse.2008.10.015, 2009
Dee, D.P., Uppala, S. M., Simmons, A. J., Berrisford, P., et al.: The ERA-Interim reanalysis: configuration and performance of the data assimilation system, Quart. J. Roy. Meteor. Soc., 137, 553–597. Doi: 10.1002/qj.828, 2011
Donlon, C.J., Martin, M., Stark, J. D., Roberts-Jones, J., and Fiedler, E.: The Operational Sea Surface Temperature and Sea Ice Analysis (OSTIA) system. Rem. Sens. of Environment, 116: 140-158. doi:10.1016/j.rse.2010.10.017, 2012.
Drange, H., and Simonsen, K.: Formulation of air-sea fluxes in the ESOP2 version of MICOM, Technical Report No. 125 of Nansen Environmental and Remote Sensing Center, 1996.
Forsberg, R. and Skourup, H.: Arctic Ocean gravity, geoid and sea-ice freeboard heights from ICESat and GRACE. *Geophys. Res. Lett.,* **32**(21), L21502. doi:10.1029/2005GL023711, 2005.
Giles, K. A., Laxon, S. W., Wingham, D. J., et al.: Combined airborne laser and radar altimeter measurements over the Fram Strait in May 2002. Remote Sensing of Environment. 111(2-3), 182-194, doi:10.1016/j.rse.2007.02.037, 2007.
Guemas, V., Wrigglesworth, E. B., Chevallier, M., et al.: A review on Arctic sea‐ice predictability and prediction on seasonal to decadal time scales. Q. J. R. Meteorolog. Soc., 142(695), dio:10.1002/qj.2401, 2014.
Heygster, G., Hendricks, S., Kaleschke, L., Maass, N., Mills, P., Stammer, D., Tonboe, R. T., and Haas, C.: *L-Band Radiometry for Sea-Ice Applications*, Final Report for ESA ESTEC Contract 21130/08/NL/EL, Institute of Environmental Physics, University of Bremen, November 2009, 219 pp, 2009.
Hunke, E. C., and Dukowicz, J. K.: An elastic-viscous-plastic model for sea ice dynamics, J. Phys. Oceanogr., 27, 1849–1867. Doi: http://dx.doi.org/10.1175/1520-0485(1997)027<1849:AEVPMF>2.0.CO:2, 1997.
Huntemann, M., Heygster, G., Kaleschke, L., Krumpen, T., Mäkynen, M., and Mrusch, M.: Empirial sea ice thickness retrieval during the freeze-up period from SMOS high incident angle observations, The Cryosphere, 8, 439-451, doi:10.5194/tc-8-439-2014, 2014
Kaleschke, L., Maaß, N., Haas, C., Hendricks, S., Heygster, G., and Tonbøe, R.: A sea-ice thickness retrieval model for 1.4 GHz radiometry and application to airborne measurements over low salinity sea-ice, The Cryosphere, 4, 583 – 592. Doi: 10.5194/tc-4-583-2010, 2010.
Kaleschke, L., Tian-Kunze, X., Maaß, N., Mäkynen, M., and Drusch, M.: Sea ice thickness retrieval from SMOS brightness temperatures during the Arctic freeze-up period. J. Geophys. Lett. 39, L05501, doi: 10.1029/2012GL050916, 2012
Kaleschke, L., Tian-Kunze, X., Maaß, N., Ricker, R., Hendricks, S., and Drusch, M.: Improved retrieval of sea ice thickness from SMOS and Cryosat-2. Proceedings of 2015 International Geoscience and Remote Sensing Symposium IGARSS. Doi: 10.1109/IGARSS.2015.7327014, 2015.
Kaleschke, L., Tian-Kunze, X., Maaß, N., et al.: SMOS sea ice product: Operational application and validation in the Barents Sea marginal ice zone. Remote Sensing of Environment, doi:10.1016/j.rse.2016.03.009, 2016.
Karl, T. R., Arguez, A., Huang, B., Lawrimore, J. H., McMahon, J. R., Menne, M. J., Peterson, T. C., Vose, R. S., and Zhang, H. -M.: Possible artifacts of data biases in the recent global surface warming hiatus. Science, 348 (6242), 1469-1472. doi: 10.1126/science.aaa5632, 2015.
Korosov, A., Counillon, F., and Johannessen, J. A.: Monitoring the spreading of the Amazon freshwater plume by MODIS, SMOS, Aquarius, and TOPAZ. J . Geophys. Res., 120, 268-283, doi:10.1002/2014JC010155, 2015.
Krishfield, R., J. Toole, A. Proshutinsky, and M. -L. Timmermans, Automated Ice-Tethered Profilers for Seawater Observations Under Pack Ice in All Seasons, *J. Atmos. Oceanic Technol.*, 25, 2091-2105, DOI: http://dx.doi.org/10.1175/2008JTECHO587.1, 2008.

Kurtz, N. T., Markus, T., Cavalieri, D. J., Sparling, L. C., Krabill, W. B., Gasiewski, A. J., and Sonntag, J. G.: Estimation of sea ice thickness distributions through the combination of snow depth and satellite laser altimetry data, J. Geophys. Res., 114, C10007, doi:10.1029/2009JC005292, 2009.

Kwok, R., and Rothrock, D.: Decline in Arctic sea ice thickness from submarine and ICESat records: 1958–2008, Geophys. Res. Lett., 36, L15501, doi:10.1029/2009GL039035, 2009.

Johnson, M., Proshutinsky A., Aksenov Y., Nguyen A. T., Lindsay R., Haas C., Zhang J., Diansky N., Kwok R., et al.: Evaluation of Arctic sea ice thickness simulated by Arctic Ocean Model Intercomparison Project models. J. Geophys. Res., 117(C8), doi:10.1029/2011JC007257, 2012.

Johannessen, J. A., Raj, R.P., Nilesen, J. E. Ø., Pripp, T., Knudsen, P., Counillon, F., Stammer, D., Bertino, L., Andersen, O. B., Serra, N., and Koldunov, N.: Toward Improved Estimation of the Dynamic Topography and Ocean Circulation in the High Latitude and Arctic Ocean: The Importance of GOCE. Surv Geophys, doi:10.1007/s10712-013-9270-y, 2014.

Johannessen, O. M., Shalina, E. V., and Miles, M. W.: Satellite evidence for an Arctic Sea ice cover in transformation, Science, 286, 1937—1939. Doi:10.1126/science.286.5446.1937, 1999.

Laxon, S., Peacock, N., and Smith, D.: High interannual variabilityof sea ice thickness in the Arctic region, Nature, 425, 947–950, doi:10.1038/nature02050, 2003.

Laxon, S. W., Giles, K. A., Ridout, A. L., Wingham, D. J., Willatt, R., Cullen, R., Kwok, R., Schweiger, A., Zhang, J., Haas, C., Hendricks, S., Krishfield, R., Kurtz, N., Farrell, S., and Davidson, M.: CryoSat-2 estimates of Arctic sea ice thickness and volume, Geophys. Res. Lett., 40, 732–737, doi:10.1002/grl.50193, 2013.

Lien, V. S., Hjøllo, S. S., Skogen, M. D., Svendsen, E., Wehde, H., Bertino, L., Counillon, F., Chevallier, M., and Garric, G.: An assessment of the added value from data assimilation on modelled Nordic Seas hydrography and ocean transports, Ocean Modelling, doi:10.1016/j.ocemod.2015.12.010, 2016.

Lisæter, K. A., G. Evensen, and S. Laxon (2007), Assimilating synthetic CryoSat sea ice thickness in a coupled ice-ocean model, J. Geophys. Res., 112, C07023, doi:10.1029/2006JC003786.

Locarnini, R., Antonov, J., and Garcia, H.: World Ocean Atlas 2005, Volume 1: Temperature, vol. 61, US Dept. of Commerce, National Oceanic and Atmospheric Administration, 2006.

Mecklenburg, S., Drusch, M., Kaleschke, L., Rodriguez-Fernandez, N., Reul, N., Kerr, Y., Font, J., Martin-Neira, M., Oliva, R., Daganzo-Eusebio, E., Grant, J. P., Sabia, R., Macelloni, G., Rautiainen, K., Fauste, J., de Rosnay, P., Munoz-Sabater, J., Verhoest, N., Lievens, H., Delwart, S., Crapolicchio, R., de la Fuente, A., and Kornberg, M.: ESA's Soil Moisture and Ocean Salinity mission: From science to operational applications, Remote Sensing of Environment, http://dx.doi.org/10.1016/j.rse.2015.12.025, 2016.

Melsom, A., Counillon, F., LaCasce, J. H., and Bertino, L.: Forecasting search areas using ensemble ocean circulation modeling. Ocean Dynamics, 62(8), 1245-1257, 2012.

Nerger, L., Hiller, W., and Schröter J.: A comparison of error subspace Kalman filters, Tellus A., 57(5), 715-735, doi: 10.1111/j.1600-0870.2005.00141.x, 2005.

Ricker, R., Hendricks, S., Helm, V., et al.: Sensitivity of CryoSat-2 Arctic sea-ice freeboard and thickness on radar-waveform interpretation, The Cryosphere, 8, 1607-1622, doi:10.5194/tc-8-1607-2014, 2014.

Rodgers, C.: Inverse methods for atmospheres: theory and practice, World Scientific, 2000.

Roemmich, D., Church, J., Gilson, J., Monselesan, D., Sutton, P., and Wijffels, S.: Unabated planetary warming and its ocean structure since 2006. *Nature Climate Change* 5, 240–245. doi:10.1038/nclimate2513, 2015.

Rothrock, D. A., Yu, Y., and Maykut, G. A.: Thinning of the Arctic sea ice cover, Geophys. Res. Lett r., 26, 3469 —3472. Doi:10.1029/1999GL010863, 1999.

Sakov, P., and Oke, P. R.: A deterministic formulation of the ensemble Kalman Filter: an alternative to ensemble square root filters. Tellus A, 60(2):361-371, doi:10.1111/j.1600-0870.2007.00299.x, 2008.

Sakov, P., Evensen, G., and Bertino, L.: Asynchronous data assimilation with the EnKF. Tellus A, 62(1), 24-29. Doi:10.1111/j.1600-0870.2009.00417.x, 2010.

Sakov, P., Counillon, F., Bertino, L., Lisæter, K. A., Oke, P. R., and Korablev, A.: TOPAZ4: an ocean-sea ice data assimilation system for the North Atlantic and Arctic. Ocean Science, 8:633-656, doi:10.5194/os-8-633-2012, 2012.

Schweiger, A., Lindsay, R., Zhang, J., Steels, M., Stern, H., and Kwok, R.: Uncertainty in modeled Arctic sea ice volume, J. Geophys. R., 116, C00D06, doi:10.1029/2011JC007084, 2012.

Serreze, M., Walsh, J., Chapin, F., Osterkamp, T., Dyurgerov, M., Romanovsky, V., Oechel, W., Morrison, J., Zhang, T., and Barry, R. G.: Observational evidence of recent changes in the northern high latitude environment, Climate Change, 46,159 — 207. Doi: 10.1023/A:1005504031923, 2000.

Shimada, K., Kamoshida, T., Itoh, M., Nishino, S., Carmack, E., McLaughlin, F., Zimmermann, S., and Proshutinsky, A.: Pacific Ocean inflow: Influence on catastrophic reduction of sea ice cover in the Arctic Ocean, Geophys. Res. Lett., 33(8), doi:10.1029/2005GL025624, 2006.

Smith, G. C., Roy, F., Reszka, M., Colan, D. S., He, Z., Deacu, D., et al.: Sea ice forecast verification in the Canadian Global Ice Ocean Prediction System. Quart. J. Roy. Meteor. Soc., doi:10.1003/qj.2555, 2015.

Steele, M., Morley, R., and Ermold, W.: PHC: A global ocean hydrography with a high-quality Arctic Ocean, J. Climate, 14, 2079–2087. Doi:http://dx.doi.org/10.1175/1520-0442(2001)014<2079:PAGOHW>2.0.CO:2, 2001.

Tian-Kunze, X., Kaleschke, L., Maaß, N., Mäkynen, M., Serra, N., Drusch, M., and Krumpen, T.: SMOS-derived sea ice thickness: algorithm baseline, product specifications and initial verification, The Cryosphere, 8, 997-1018, doi:10.5194/tc-8-997-2014, 2014.

Tilling, R. L., Ridout, A., and Shepherd, A.: Near real time Arctic sea ice thickness and volume from CryoSat-2, The Cryosphere Discuss., doi:10.5194/tc-2016-21, 2016.

Toole, J.M., R.A. Krishfield, M.-L. Timmermans, and A. Proshutinsky. 2011. The Ice-Tethered Profiler: Argo of the Arctic. *Oceanography* 24(3):126–135, http://dx.doi.org/10.5670/oceanog.2011.64, 2011

Woodgate, R. A., Weingartner, T. J., and Lindsay, R.: Observed increases in Bering Strait oceanic fluxes from the Pacific to the Arctic from 2001 to 2011 and their impacts on the Arctic Ocean water column, Geophys. Res. Lett., 39, L24603, doi:10.1029/2012GL054092, 2012.

Xie, J., Bertino, L., Counillon, F., Lisæter, K. A., and Sakov, P.: Quality assessment of the TOPAZ4 reanalysis in the Arctic over the period 1991–2013, Ocean Sci. Discuss., doi:10.5194/os-2016-38, in review, 2016.

Yang, Q., Losa, S. N., Losch, M., Tian-Kunze, X., Nerger, L., Liu, J., Kaleschke, L., and Zhang, Z.: Assimilating SMOS sea ice thickness into a coupled ice-ocean model using a local SEIK filter, J. Geophys. Res. Oceans, 119, doi:10.1002/2014JC009963, 2014.

Yang, Q., Losch, M., Jung, T., and Nerger, L.: Taking into account atmospheric uncertainty improve sequential assimilation of SMOS sea ice thickness data in an ice-ocean model, , *J. Atmos. Oceanic Technol.*, doi:http://dx.doi.org/101175/JTECH-D-15-0176.1, 2016.

Zygmuntowska, M., Rampal, P., Ivanova, N., and Smedsrud, L. H.: Uncertainties in Arctic sea ice thickness and volume: new estimates and implications for trends. The Cryosphere, 8, 705–720, doi:10.5194/tc-8-705-2014, 2014.

Table 1. Overview of assimilated observations in each assimilation cycle of the present TOPAZ system. All observations are retrieved from http://marine.copernicus.eu.

Type	Spacing	Resolution	Provider
SLA	Track	-	CLS
SST	Gridded	5 km	OSTIA from UK Met Office
In-situ T	Point	-	Ifremer + other
In-situ S	Point	-	Ifremer + other
ICEC	Gridded	10 km	OSISAF
Ice drift	Gridded	62.5 km	OSISAF

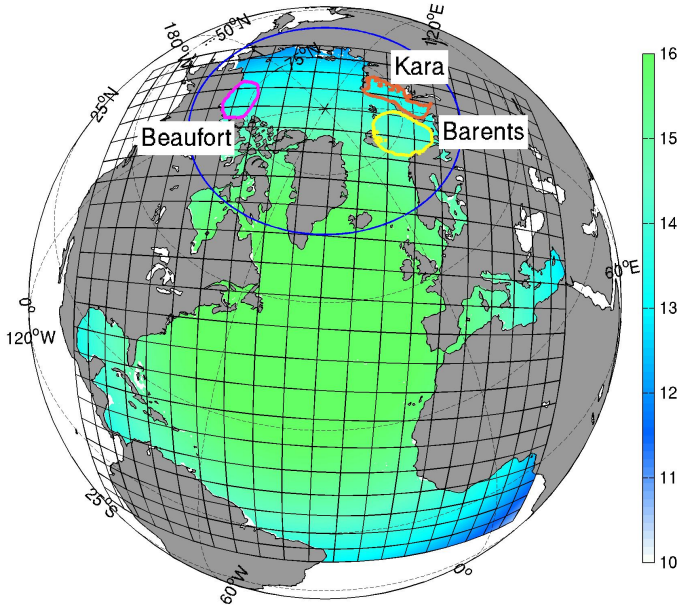

Fig. 1 TOPAZ model domain and horizontal grid resolution (km) with color shading. The blue line delimits the focused Arctic region (north of 63°N) and other color lines delimit the three marginal seas discussed in this study.

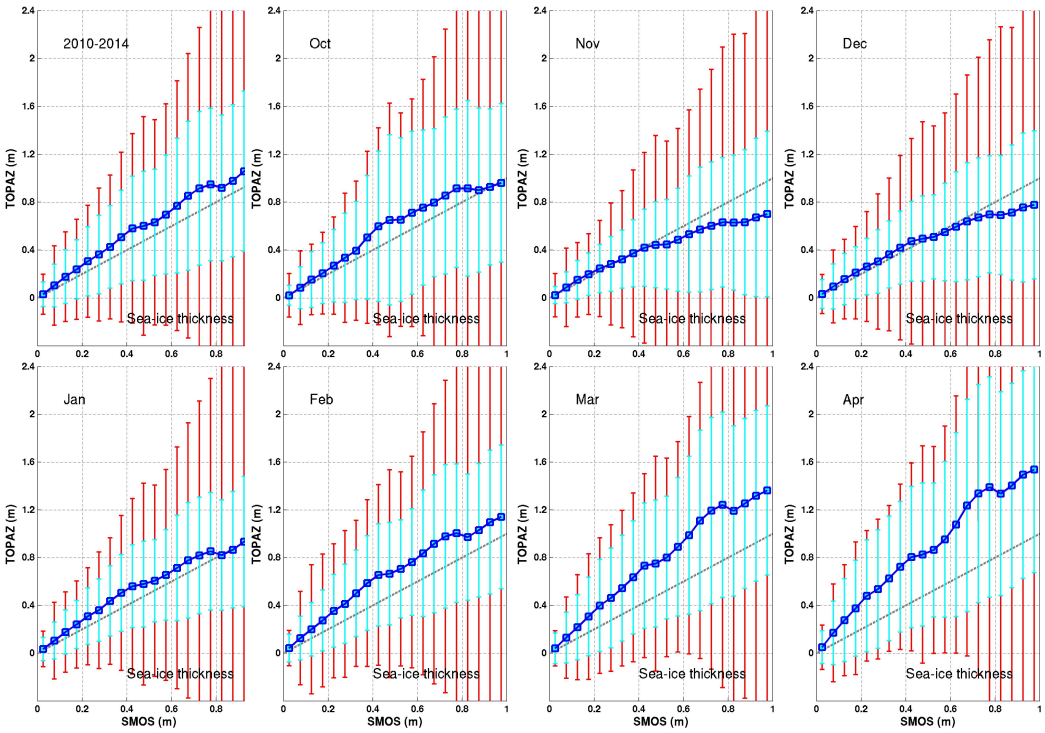

Fig. 2 Conditional expectations of TOPAZ versus SMOS-Ice (with bin of 5 cm) for the period 2010-2014 and for each month. The cyan error-bars correspond to the RMSD against all observations within each bin. The red error-bars correspond to averaged standard deviations of observation error. The gray dashed line denotes the line y=x.

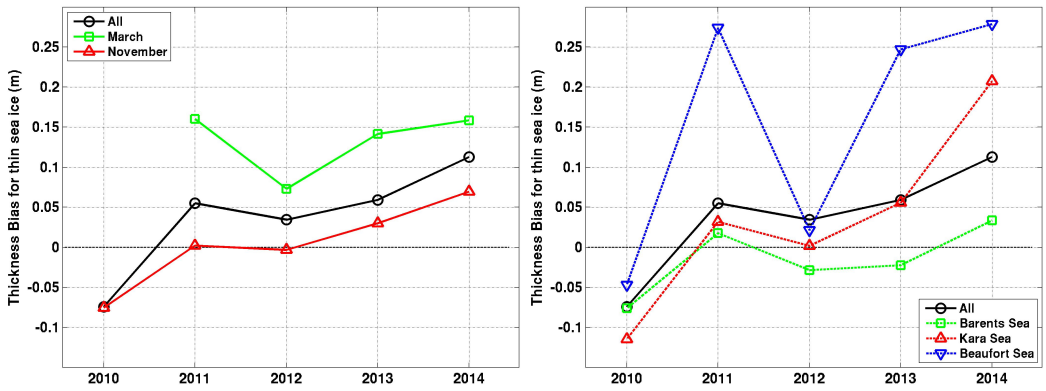

Fig. 3 Yearly thickness biases of thin sea ice from TOPAZ compared to SMOS-Ice observations. The black line represents the yearly mean bias. **Left**: the green (red) line represents the mean bias for March (November) of each year. **Right**: the colored lines represent the biases in the Barents Sea, the Kara Sea, and the Beaufort Sea.

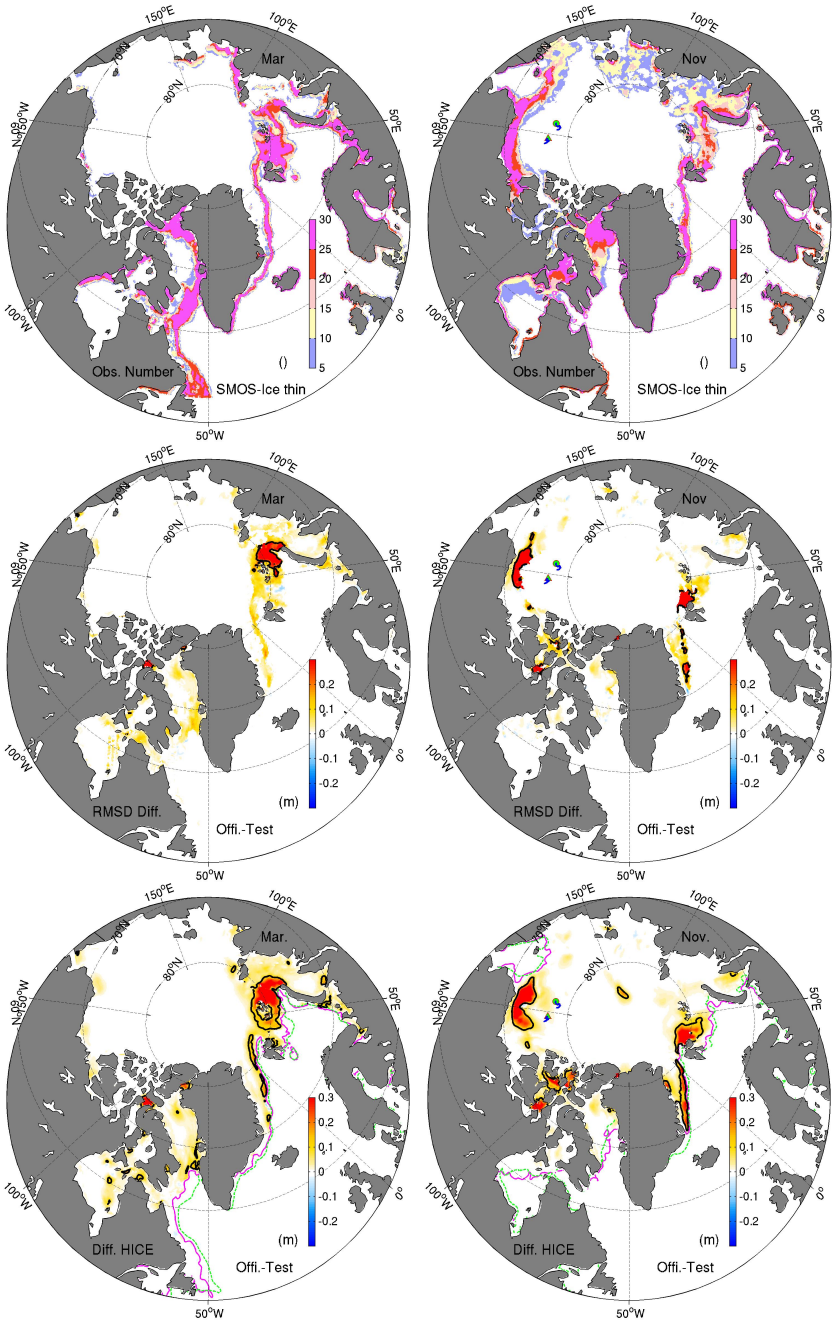

Fig. 4 **Top Row**: SMOS-Ice data numbers can be assimilated in March (left) and in November (right) of 2014. **Middle Row**: Difference of RMSDs for the thin sea-ice thicknesses between Official Run and Test Run in March (*left*) and in November (*right*). **Bottom Row:** Difference of mean ice thicknesses between the two runs. The black line denotes the 0.2 m isoline, the green (pink) line is the 15% concentration isoline from OSISAF (Official Run). The marker of circle (triangle) represents the position of sea-ice buoy *2013F* (*2014F*) at First November 2014.

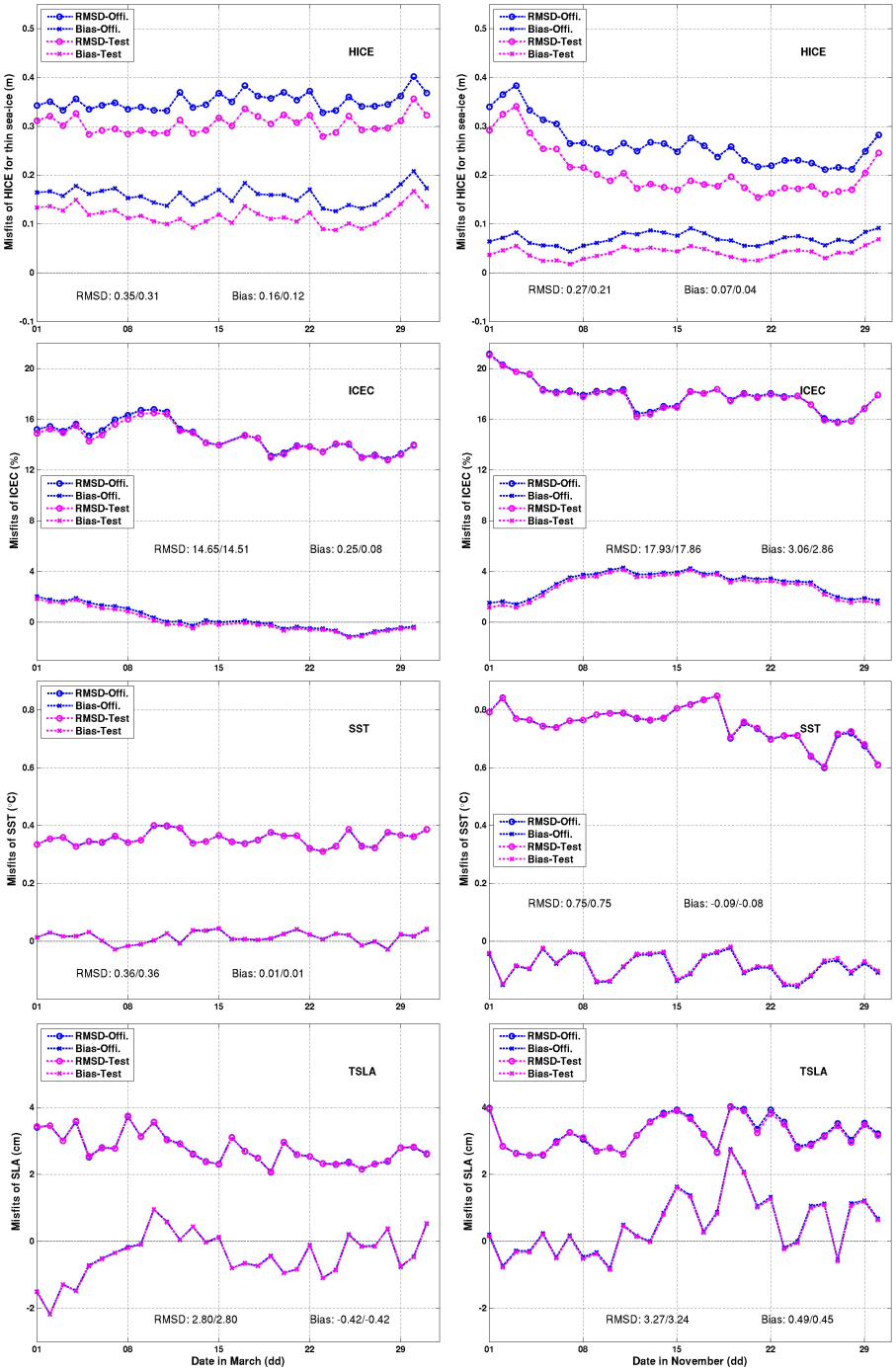

Fig. 5 Daily time series of the bias (marked with crosses) and the RMSD (marked with circles) in the whole Arctic for the Official Run (in blue) and the Test Run (in purple) for different variables in March (Left) and November (Right).

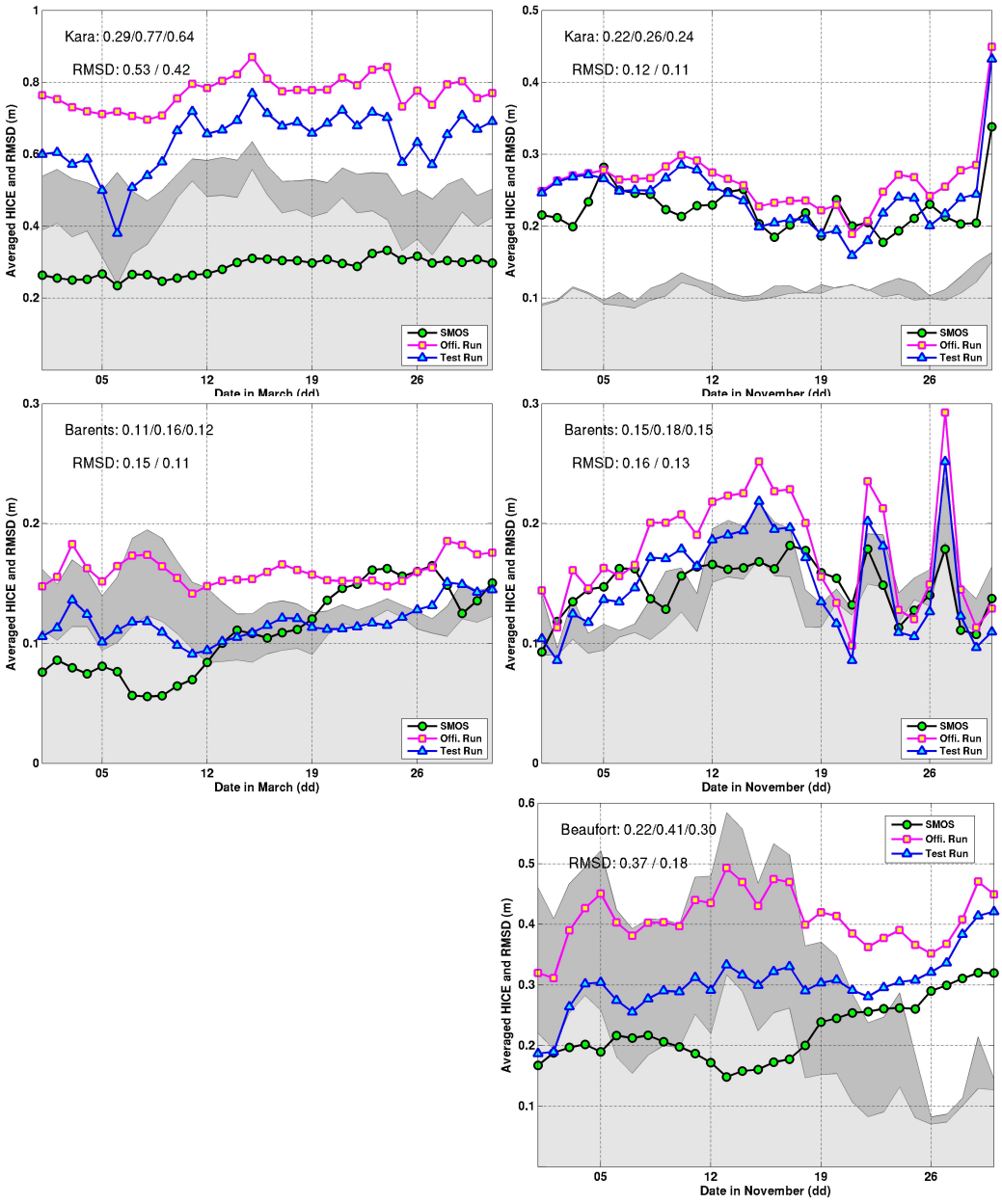

Fig. 6 Daily time series of the mean thickness of thin sea-ice in the Kara Sea (top row), the Barents Sea (middle row) and Beaufort Sea (bottom row) for March (*left*) and November (*right*). The light (dark) gray shading is the daily spatial RMSD of thin sea ice in the Test Run (Official Run).

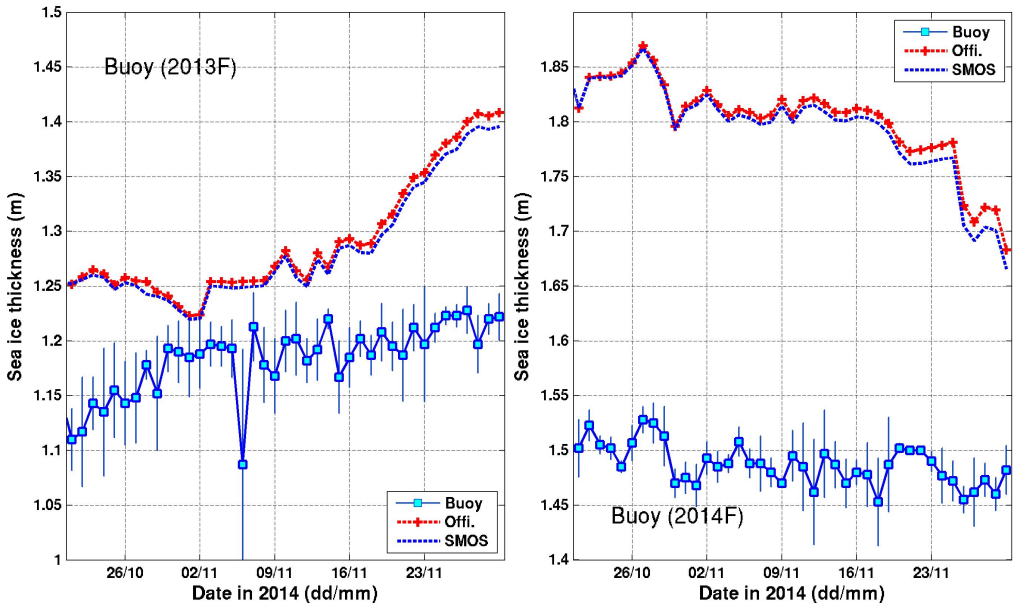

Fig 7. Daily time series of sea ice thickness from Official Run (crossed red line) and Test Run (dashed blue line) during the period from 21th October to 30 November compare with the sea-ice buoy measurements (squared blue line) with its daily standard deviation as the error bar. The buoy data are from autonomous ice mass balance (IMB; http://imb.erdc.dren.mil), and their drift trajectories in November 2014 are shown in Fig. 4. **Left**: Buoy *2013F*; **Right**: *Buoy 2014F*.

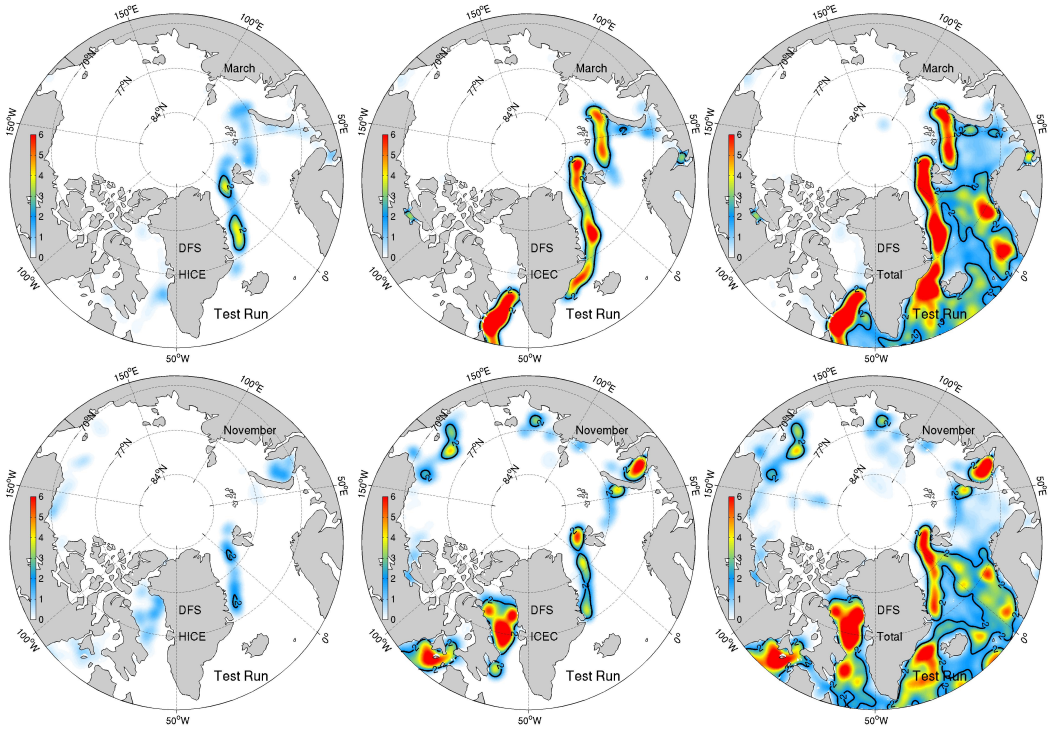

Fig. 8 Monthly averaged Degrees of Freedom for Signal (DFS) from the Test Run in March (*upper*) and in November (*lower*) for SMOS-Ice sea ice thickness (left column), sea ice concentration (middle column), and the total DFS of all ice and ocean observations (right column). The black line denotes the isoline of DFS equal to 2.

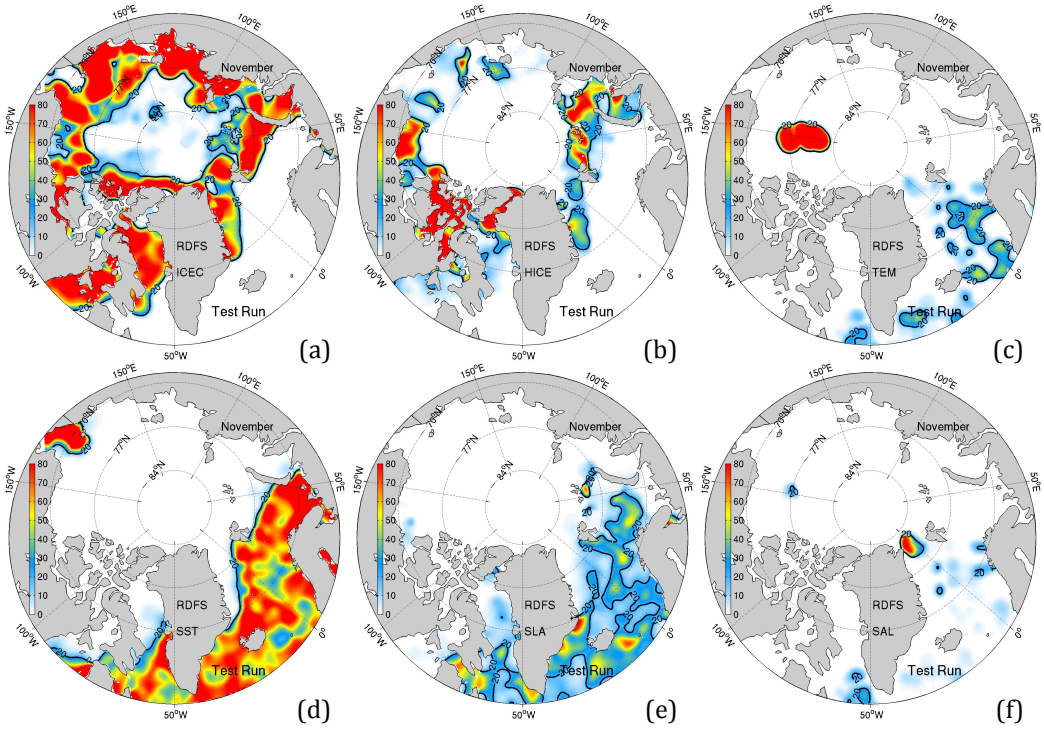

Fig. 9 Relative contributions of each observational data set in the total DFS during March 2014. Panel (a) is for sea ice concentration; (b) ice thickness from SMOS-Ice; (c) temperature profiles; (d) SST; (e) along-track Sea Level Anomaly; (f) salinity profiles. The black line is the 20% isoline.

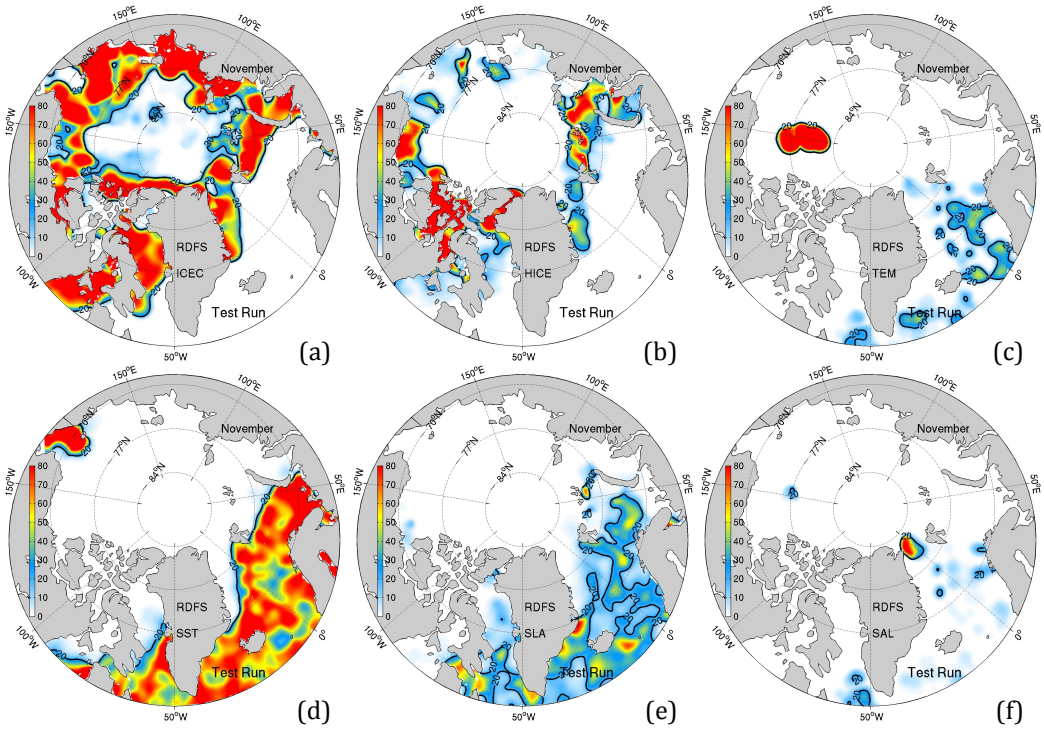

Fig. 10 Same as Figure 10 for November 2014